

# Generation of Dicke states using adiabatic passage

K. Toyoda, T. Watanabe, T. Kimura, S. Nomura, S. Haze, S. Urabe

*Graduate School of Engineering Science, Osaka University,*

*1-3 Machikaneyama, Toyonaka, Osaka, Japan*

(Dated: April 3, 2024)

## Abstract

Entangled states of two ions are realized by using an adiabatic process. Based on the proposal by Livingston and Vitanov [1], we have generated Dicke states in optical qubits of two  $^{40}\text{Ca}^+$  ions by applying frequency-chirped optical pulses with time-dependent envelopes to perform rapid adiabatic passage on sideband transitions. One of the biggest advantages of adiabatic approaches is their robustness against variations in experimental parameters, which is verified by performing experiments for different pulse widths or peak Rabi frequencies. Fidelities exceeding 0.5, which is the threshold for inseparable states, are obtained over wide ranges of parameter values.

PACS numbers: 03.67.Bg, 37.10.Ty

## I. INTRODUCTION

Multipartite entanglement plays a central role in quantum information science. Entangled states have been generated and studied in various systems, including photons and trapped ions [2–6]. Of multipartite entangled states, a set of states known as Dicke states [7] has recently been attracting interest. Dicke states are entangled states that are symmetric with respect to particle permutations. They are defined as

$$|D_N^{(m)}\rangle \equiv \binom{N}{m}^{-1/2} \sum_k P_k(|\downarrow^{\otimes(N-m)}\uparrow^{\otimes m}\rangle), \quad (1)$$

where  $N$  and  $m$  are respectively the number of particles and excitations and  $\sum_k P_k(\dots)$  indicates the sum over all particle permutations. W states, a subset of Dicke states with a single excitation, have been produced and investigated using up to eight trapped ions [2]. Dicke states of up to six photons have been generated and their unique characteristics, such as entanglement persistency against photon loss and projective measurements, have been studied [5, 6, 8, 9].

Linington and Vitanov [1] proposed a relatively simple and effective method for generating Dicke states in a string of ions that utilizes frequency-chirped optical pulses. The method described in Ref. [1] can be used to generate Dicke states for arbitrary numbers of particles and excitations. For small numbers of excitations  $m$ , resonant pulses can also be used to produce Dicke states  $|D_N^{(m)}\rangle$ , although in this case perfect fidelity is possible only when  $m = 1$ . Hume *et al.* [10] analyzed the fidelity attainable by a method using resonant pulses and experimentally demonstrated it using two  $^{25}\text{Mg}^+$  ions and an ancillary  $^{27}\text{Al}^+$  ion.

In this article we report the generation of an entangled state of two ions,  $|D_2^{(1)}\rangle = (1/\sqrt{2})(|\downarrow\uparrow\rangle + |\uparrow\downarrow\rangle)$ , by using rapid adiabatic passage (RAP) [11–13] in a sideband transition of  $S_{1/2}-D_{5/2}$  of  $^{40}\text{Ca}^+$ . We also analyze the effects of using optical pulses with time-dependent envelopes for RAP. Such pulses produce time-dependent AC Stark shifts that may result in violation of adiabaticity. One advantage of using adiabatic passage to generate Dicke states is its robustness against parameter variations. Using an AC-Stark-shift compensator that cancels time-dependent AC Stark shifts, the robustness of entanglement generation is verified by varying the width and peak intensity of the optical pulse used for RAP. The method employed here can be extended to generate larger Dicke states with more particles and excitations.

## II. PRINCIPLES

Fig. 1 depicts the basic concept for generating Dicke states using RAP. The internal states of two ions and the motional Fock states of their axial center-of-mass (COM) mode are respectively denoted as  $|s_1 s_2\rangle$  and  $|n\rangle$ , where  $s_1(s_2) = \downarrow, \uparrow$  represents a qubit state of each ion and  $n$  denotes the motional quantum number.

The ions are initially prepared in a motional Fock state  $|\downarrow\downarrow\rangle|1\rangle$  using either  $\pi$  pulses or RAP pulses on the blue (red) sideband and a carrier transition that are addressed to only one of the ions; e.g., a blue sideband  $\pi$  pulse followed by a carrier  $\pi$  pulse, both of which are addressed to the first ion, to transfer the ions as  $|\downarrow\downarrow\rangle|0\rangle \rightarrow |\uparrow\downarrow\rangle|1\rangle \rightarrow |\downarrow\downarrow\rangle|1\rangle$ .

An entangling operation is performed with a laser beam tuned closely to  $\omega_L = \omega_0 - \omega_v$ , which excites the red sideband transition, where  $\omega_L$  ( $\omega_0$ ) is the laser (atomic resonance) frequency and  $\omega_v$  is the secular frequency of the axial COM mode. This preserves the total number of excitations  $N_e = N_a + n$ , where  $N_a$  is the number of atoms in  $|\uparrow\rangle$ ; hence,  $|\downarrow\downarrow\rangle|1\rangle$  is coupled only to  $|\downarrow\uparrow\rangle|0\rangle$  and  $|\uparrow\downarrow\rangle|0\rangle$ , and the relevant states form a V-shape diagram.

When the ions are excited by a single laser, the time dependences of the Rabi frequency for each ion are the same up to a proportionality factor. In addition, the detuning for each ion will also be the same when the difference in level shifts due to Zeeman or Stark effects can be neglected. In such a case, the system can be further simplified by a unitary transformation in the upper manifold with  $n = 0$  spanned by  $|\downarrow\uparrow\rangle|0\rangle$  and  $|\uparrow\downarrow\rangle|0\rangle$ , and it becomes equivalent to a two-state system and an uncoupled (dark) state (right diagram in Fig. 1(a)). This is one of the simplest examples of a more general prescription known as the Morris–Shore transformation [14, 15]. If the two ions have the Rabi frequencies of the same time dependence, the two-state system will consist of  $|\downarrow\downarrow\rangle|1\rangle$  and a Dicke state (or a Bell state)  $|D_2^{(1)}\rangle|0\rangle = (1/\sqrt{2})(|\downarrow\uparrow\rangle + |\uparrow\downarrow\rangle)|0\rangle$ , with the uncoupled state being equal to another Bell state with the same  $N_a$ ,  $(1/\sqrt{2})(|\downarrow\uparrow\rangle - |\uparrow\downarrow\rangle)|0\rangle$ .

Thus, starting from  $|\downarrow\downarrow\rangle|1\rangle$ , either a  $\pi$  pulse or RAP on the red sideband transition can be used to transfer the population to the desired final state  $|D_2^{(1)}\rangle|0\rangle$ . Fig. 1(b) shows the adiabatic potentials for the case of RAP and plots the energy levels with different detunings for the red sideband pulse. The population follows the lower curve to be adiabatically transferred from  $|\downarrow\downarrow\rangle|1\rangle$  to  $|D_2^{(1)}\rangle|0\rangle$ . (Here, the Rabi frequencies are assumed to be constant for simplicity, while it is usually varied in actual experiments. )

This scheme can be extended to more ions  $N > 2$  and more excitations  $N_e > 1$  to produce

$|D_N^{(N_e)}\rangle|0\rangle$ . The latter extension requires extending the Morris–Shore transformation to multilevel ladders [15]; in this case, the initial state  $|\downarrow \dots \downarrow\rangle|N_e\rangle$  is coupled to the final state by a ladder with  $N_e + 1$  energy levels. With unitary operations induced by resonant optical pulses, the dynamics in this multilevel diagram never produce a unit population in the final state  $|D_N^{(N_e)}\rangle|0\rangle$  [10, 16], whereas when using RAP, such an objective can be accomplished, at least under ideal conditions [1].

### III. EXPERIMENTAL PROCEDURE

The trapping system and laser setup used in the present study are similar to those described in [17]. In brief, we use two  $^{40}\text{Ca}^+$  in a linear trap with center-of-mass frequencies of  $(\omega_x, \omega_y, \omega_z)/2\pi = (2.4, 2.2, 0.7)$  MHz. As the qubit states  $|\downarrow\rangle \equiv |S_{1/2}, m_J = -1/2\rangle$  and  $|\uparrow\rangle \equiv |D_{5/2}, m_J = -3/2\rangle$  are used, and the transition between them is excited by a titanium–sapphire laser beam with a wavelength of 729 nm. The envelopes and frequencies of the optical pulses used for RAP are controlled by an acousto-optic modulator (AOM) in a double-pass configuration. Linear frequency chirping of the rf for the AOM is performed using a direct digital synthesizer. The pulse envelope is varied by using a mixer with a digital-to-analog converter as an input. Both the direct digital synthesizer and the digital-to-analog converter are controlled by a field-programmable gate array.

Individual addressing is required to prepare motional Fock states in advance to the entangling operation, which is here done using AC Stark shifts generated by a 854 nm beam that is off resonance with the  $^2D_{5/2} \rightarrow ^2P_{3/2}$  transition. This beam, which has a  $1/e^2$  intensity radius of 15  $\mu\text{m}$ , is applied to the two ions at 45 degrees to their axis, with a small offset from their center to produce different shifts for the ions. Typical shifts for the two ions are  $\sim(10, 100)$  kHz, respectively.

After Doppler cooling and ground-state cooling of axial COM and stretch modes, average quantum numbers  $(\bar{n}_{\text{COM}}, \bar{n}_{\text{st}}) \sim (0.06, 0.06)$  are obtained, respectively. A motional Fock state  $|n = 1\rangle$  is prepared by applying a blue sideband and a carrier  $\pi$  pulse in series to one ion using the individual addressing technique described above. An entangling operation is then performed by applying a chirped pulse to the red sideband transitions of both ions. A chirp width of 200 kHz typically used; i.e., the detuning is swept from  $-100$  to  $+100$  kHz.

We also use an AC-Stark-shift compensator in experiments to verify the robustness of Dicke state generation (see §VI). To realize this, we use another AOM in a single-pass configuration.

Two RF signals with independently variable frequencies and powers, one of which is for direct excitation and the other for AC-Stark-shift compensation, are combined and fed to this AOM. The output of this AOM is directed into a single-mode optical fiber and then into the above-mentioned double-pass AOM system, and it is applied to ions.

#### IV. RESULT OF DICKE STATE GENERATION

The fidelity for generating a Dicke state  $|D_2^{(1)}\rangle$ ,  $F \equiv \langle D_2^{(1)} | \rho | D_2^{(1)} \rangle = (\rho_{\downarrow\uparrow, \downarrow\uparrow} + \rho_{\uparrow\downarrow, \uparrow\downarrow})/2 + \text{Re}(\rho_{\downarrow\uparrow, \uparrow\downarrow})$ , is analyzed by performing global rotations and projective measurements. The sum of the diagonal elements,  $\rho_{\downarrow\uparrow, \downarrow\uparrow} + \rho_{\uparrow\downarrow, \uparrow\downarrow}$  is estimated by performing projective measurements immediately after the RAP pulse. The result is shown in Fig. 2(a). The histogram of fluorescence counts obtained by using a 397-nm laser beam is plotted. From this,  $\rho_{\downarrow\uparrow, \downarrow\uparrow} + \rho_{\uparrow\downarrow, \uparrow\downarrow} = 0.74 \pm 0.06$  is obtained.

The term containing off-diagonal elements,  $\text{Re}(\rho_{\downarrow\uparrow, \uparrow\downarrow})$  is estimated by parity measurements after applying a  $\pi/2$  pulse with a variable phase. The parity after applying a  $\pi/2$  pulse with phase  $\phi$  is expressed as follows.

$$\begin{aligned} \Pi(\phi) &\equiv \text{tr}(\hat{\Pi}R_{\pi/2}(\phi)^\dagger \hat{\rho} R_{\pi/2}(\phi)) \\ &= 2(\text{Re}(\rho_{\downarrow\uparrow, \uparrow\downarrow}) - \text{Re}(\rho_{\downarrow\downarrow, \uparrow\uparrow}) \cos 2\phi + \text{Im}(\rho_{\downarrow\downarrow, \uparrow\uparrow}) \sin 2\phi), \end{aligned}$$

where  $\hat{\Pi} \equiv |\downarrow\downarrow\rangle\langle\downarrow\downarrow| + |\uparrow\uparrow\rangle\langle\uparrow\uparrow| - |\downarrow\uparrow\rangle\langle\downarrow\uparrow| - |\uparrow\downarrow\rangle\langle\uparrow\downarrow|$  is the parity operator.  $R_{\pi/2}(\phi)$  represents the rotation operation with a  $\pi/2$  pulse with phase  $\phi$ . In cases with perfect fidelity,  $\Pi(\phi)$  is unity regardless of  $\phi$ . In realistic cases, the offsets of sinusoidal fits to the measured values give the values of  $2\text{Re}(\rho_{\downarrow\uparrow, \uparrow\downarrow})$ .

Fig. 2(b) shows parity measurement results. Open circles represent measured values of  $\Pi(\phi)$  and the solid curve is a sinusoidal fit with period  $\pi$  to the measured values. From this,  $2\text{Re}(\rho_{\downarrow\uparrow, \uparrow\downarrow}) = 0.58 \pm 0.02$  is obtained. Combined with the above result for the diagonal matrix elements, the fidelity for Dicke state generation is estimated to be  $F = 0.66 \pm 0.03$ .

$|D_2^{(1)}\rangle$  can be transferred to  $(1/\sqrt{2})(|\downarrow\downarrow\rangle + |\uparrow\uparrow\rangle)$  with a  $\pi/2$  pulse, and parity measurement after such a transfer may also give an indication of entanglement. The filled circles in Fig. 2(b) represent parity after Dicke state generation followed by two  $\pi/2$  pulses with the phase of the second varied. The sinusoidal oscillation with period  $\pi$  indicates the presence of  $(1/\sqrt{2})(|\downarrow\downarrow\rangle + |\uparrow\uparrow\rangle)$  after the first  $\pi/2$  pulse. By combining this result with that for one  $\pi/2$  pulse described above, we estimate the

fidelity for generation of  $(1/\sqrt{2})(|\downarrow\downarrow\rangle + |\uparrow\uparrow\rangle)$  to be  $0.64 \pm 0.04$ .

## V. EFFECTS OF AC STARK SHIFTS

The method used here for generating Dicke states using RAP on sideband transitions requires pulses with time-dependent envelopes to perform efficient population transfer. As is well known, when intense optical pulses are applied to sideband transitions they produce large AC Stark shifts and can cause undesirable effects such as qubit-phase rotations [18]. In the sideband RAP case treated here, relevant adiabatic potentials may be deformed in unexpected ways and adiabaticity may be violated. This was avoided in the result presented above by selecting sets of parameter values such that the dynamics is not greatly affected by diabatic transitions. However, if we consider robustness against variation of parameters such as the pulse width and the peak Rabi frequency, which is one of the biggest advantages of the adiabatic method described here, we should manage AC Stark shifts appropriately.

We calculated adiabatic potentials and considered adiabaticity in the case of Dicke-state generation using sideband RAP. The calculation is based on the following time-dependent Hamiltonian in a rotating frame.

$$H(t) = -\hbar\delta(t) \sum_{j=1}^2 |\uparrow\rangle_j \langle\uparrow|_j + \hbar\omega_\nu \hat{a}^\dagger \hat{a} \\ + \sum_{j=1}^2 \left[ \frac{\hbar\Omega(t)}{2} \hat{\sigma}_{x,j} + \frac{\eta\hbar\Omega(t)}{2} (\hat{\sigma}_{+,j} \hat{a} + h.c.) \right]$$

Here,  $|s\rangle_j$  ( $s = \downarrow, \uparrow$ ) are state vectors for the  $j$ th ion,  $\hat{\sigma}_{+,j} \equiv |\uparrow\rangle_j \langle\downarrow|_j$ , and  $\hat{\sigma}_{x,j} \equiv |\uparrow\rangle_j \langle\downarrow|_j + |\downarrow\rangle_j \langle\uparrow|_j$ .  $\Omega(t)$  is the time-dependent Rabi frequency for carrier transitions, and  $\delta(t)$  is the detuning from their resonance.  $\eta$  and  $\hat{a}$  are respectively the Lamb–Dicke parameter and the annihilation operator for the axial COM mode.

We chose the following five basis states for the calculation,  $|\downarrow\downarrow\rangle|0\rangle$ ,  $|\downarrow\downarrow\rangle|1\rangle$ ,  $|D\rangle|0\rangle$ ,  $|D\rangle|1\rangle$ , and  $|\uparrow\uparrow\rangle|0\rangle$ , where  $|D\rangle$  represents  $|D_2^{(1)}\rangle = (1/\sqrt{2})(|\uparrow\uparrow\rangle + |\uparrow\downarrow\rangle)$  [see Fig. 3(a)]. These consist of the two states  $|\downarrow\downarrow\rangle|1\rangle$  and  $|D\rangle|0\rangle$ , which are connected to each other by red sideband RAP, and states that are directly connected to these two states by carrier excitation. The laser is assumed to illuminate both ions equally. In that case, the antisymmetric Bell state  $(1/\sqrt{2})(|\downarrow\uparrow\rangle - |\uparrow\downarrow\rangle)$  becomes uncoupled with other internal states and can be excluded from consideration [14, 15]. The existence of  $|\uparrow\uparrow\rangle|1\rangle$  can be neglected since it is only indirectly coupled with  $|\downarrow\downarrow\rangle|1\rangle$  via  $|D\rangle|1\rangle$

through off-resonant carrier couplings. In fact, even  $|\downarrow\downarrow\rangle|0\rangle$  and  $|\uparrow\uparrow\rangle|0\rangle$  can be neglected when calculating energy shifts, since the AC Stark shifts of  $|D\rangle|0\rangle$  due to the couplings with those states exactly cancel each other and have negligible effects. Here, we consider these states for the sake of completeness. Therefore, the only non-negligible shift originates from the coupling between  $|\downarrow\downarrow\rangle|1\rangle$  and  $|D\rangle|1\rangle$ .

Fig. 3(b) shows the time dependence of the Rabi frequency (solid curve) and detuning (dashed curve) of the assumed optical pulse. The Rabi frequencies represent those for the carrier transition. Fig. 3(c) shows the adiabatic potentials for relevant dressed states (solid curves), obtained by diagonalizing a Hamiltonian derived from the one given above. The two potentials roughly correspond to the bare states  $|\downarrow\downarrow\rangle|1\rangle$  and  $|D\rangle|0\rangle$ , where  $|D\rangle \equiv |D_2^{(1)}\rangle$ . (The quantum number of the optical field is omitted for simplicity.)

The bare-state potentials for  $|\downarrow\downarrow\rangle|1\rangle$  and  $|D\rangle|0\rangle$  intersect at the center (about 0.3 ms), where the adiabatic potentials for the dressed states approach each other, as expected. However, they also approach each other at  $\sim 0.11$  ms, which is not expected in the case of RAP in two-level systems. Under some conditions, diabatic transitions could occur at such points, reducing the fidelity.

The probability for diabatic transitions from state  $|i(t)\rangle$  to  $|j(t)\rangle$  is estimated to be [19]

$$p_{i \rightarrow j} \lesssim \max \left| \frac{\alpha_{ji}(t)}{\omega_{ji}(t)} \right|^2,$$

where  $\alpha_{ji}(t) \equiv \langle j(t) | (d/dt) | i(t) \rangle$  and  $\omega_{ji}(t) \equiv [\varepsilon_j(t) - \varepsilon_i(t)]/\hbar$ , with  $\varepsilon_i(t)$  being the adiabatic potential for  $|i(t)\rangle$ . In short, the probability is determined by the maximum value of  $|\alpha_{ji}(t)/\omega_{ji}(t)|^2$ . Fig. 3(d) shows the calculated values of  $|\alpha_{ji}(t)/\omega_{ji}(t)|^2$ . At points near 0.11 ms, where the adiabatic potentials approach each other, this value has a local maximum, which indicates that adiabaticity is about to be violated. At slightly higher intensities, the probability of diabatic transitions may become fatally large.

For comparison, potentials for an ideal case when the carrier couplings are omitted are also calculated. The dashed curves in Fig. 3(c) are calculated potentials for when the matrix elements for all the carrier couplings ( $|\downarrow\downarrow\rangle|0\rangle$ - $|D\rangle|0\rangle$ ,  $|\uparrow\uparrow\rangle|0\rangle$ - $|D\rangle|0\rangle$ ,  $|\downarrow\downarrow\rangle|1\rangle$ - $|D\rangle|1\rangle$ ) are set to be zero. These potentials correspond to the case in which the energy shifts due to the carrier couplings are perfectly compensated by the use of an AC-Stark-shift compensator (see the next section). They have clean shapes and there is only one point where they approach each other. Correspondingly, as shown by the dashed curve in Fig. 3(d),  $|\alpha_{ji}(t)/\omega_{ji}(t)|^2$  peaks only at the center, where the adiabaticity is easily satisfied since the Rabi frequency is a maximum at that point.

## VI. VERIFICATION OF ROBUSTNESS OF DICKE STATE GENERATION

Adiabaticity can be maintained by performing AC-Stark-shift compensation [18]. This can be done by applying another optical pulse such that the AC Stark shift that it produces nearly cancels the original shift. Using the AC-Stark-shift compensator described in §III, we experimentally verified the robustness of Dicke state generation against parameter variations. The compensator is used during both the blue sideband pulse in the Fock state preparation process and the red sideband RAP pulse. It is detuned in the opposite direction to the main beam for direct excitation in each period, and the absolute value of its detuning is set around a value determined by the power ratio of the two beams such that the two shifts nearly cancel each other. Here, the optical power of the compensator is set to  $\sim 60\%$  of the main beam; accordingly, the absolute value of the detuning is centered on  $\sim 400$  kHz.

The fidelity measurement results for when the peak Rabi frequency and the pulse width are varied are indicated by the circles in Fig. 4(a) and (b), respectively. In both cases, the fidelity exceeds 0.5 over wide variations in the parameters (0.5 represents the inseparability criterion for two-particle entangled states [20]).

## VII. DISCUSSION OF FIDELITY

There are several possible causes for the fidelity of Dicke state generation being limited to below 0.66. The error consists mainly of that produced when preparing motional Fock states and in the entangling operation with RAP. The causes for the former include insufficient cooling to the motional ground state and an addressing error, and the causes of the latter include phase relaxation processes due to fluctuations in the laser frequency and magnetic field and fluctuations in residual AC Stark shifts due to beam jitter.

To analyze such infidelity factors, the values of  $\rho_{\downarrow\uparrow,\downarrow\uparrow} + \rho_{\uparrow\downarrow,\uparrow\downarrow}$  and  $2\text{Re}(\rho_{\downarrow\uparrow,\uparrow\downarrow})$ , which respectively reflect the diagonal and off-diagonal density matrix elements, are shown in Fig. 4 (as crosses and asterisks, respectively). Relatively high values are obtained for the former, whereas the latter is limited to below 0.5 over both parameter ranges and it decays with increasing pulse width. Based on these facts, we speculate that the error generated in preparing motional Fock states is not significant, since otherwise we would observe a large reduction in the diagonal matrix elements. We can therefore conclude that the infidelity factors are mainly associated with the entangling

operation using RAP. We speculate that phase relaxation processes during the entangling operation mainly cause the infidelity, which is consistent with the decay with increasing pulse width. We expect that the fidelity can be improved by using resonant pulses with improved 729-nm laser linewidths (currently  $\lesssim 400$  Hz) and using transitions that are less sensitive to the magnetic field, such as  $S_{1/2}(m_J = -1/2) - D_{5/2}(m_{J'} = -1/2)$ .

## VIII. CONCLUSION

We have demonstrated generation of entangled states using an adiabatic method and demonstrated the robustness of the generation process against parameter variations. The method described here can be extended to larger numbers of particles and excitations. Recently, Wieczorek *et al.* [6] have shown experimentally that entangled states of inequivalent classes are obtained from six-photon Dicke states  $|D_6^{(3)}\rangle$  via projection measurements on a few of their qubits. In a similar way, large atomic Dicke states generated by methods similar to that described here may be used as entanglement resources for quantum information processing applications.

## ACKNOWLEDGEMENTS

This work is supported by MEXT Kakenhi ‘‘Quantum Cybernetics’’ Project and the JSPS through its FIRST Program.

- 
- [1] I. E. Lington and N. V. Vitanov, *Phys. Rev. A* **77**, 010302 (2008).
  - [2] H. Häffner, W. Hänsel, C. F. Roos, J. Benhelm, D. Chek-al kar, M. Chwalla, T. Körber, U. D. Rapol, M. Riebe, P. O. Schmidt, C. Becher, O. Gühne, W. Dür, and R. Blatt, *Nature* **438**, 643 (2005).
  - [3] D. Leibfried, E. Knill, S. Seidelin, J. Britton, R. B. Blakestad, J. Chiaverini, D. B. Hume, W. M. Itano, J. D. Jost, C. Langer, R. Ozeri, R. Reichle, and D. J. Wineland, *Nature* **438**, 639 (2005).
  - [4] R. Blatt and D. Wineland, *Nature* **453**, 1008 (2008).
  - [5] R. Prevedel, G. Cronenberg, M. S. Tame, M. Paternostro, P. Walther, M. S. Kim, and A. Zeilinger, *Phys. Rev. Lett.* **103**, 020503 (2009).
  - [6] W. Wiecek, R. Krischek, N. Kiesel, P. Michelberger, G. Tóth, and H. Weinfurter, *Phys. Rev. Lett.* **103**, 020504 (2009).

- [7] R. H. Dicke, Phys. Rev. **93**, 99 (1954).
- [8] M. Eibl, N. Kiesel, M. Bourennane, C. Kurtsiefer, and H. Weinfurter, Phys. Rev. Lett. **92**, 077901 (2004).
- [9] N. Kiesel, C. Schmid, G. Toth, E. Solano, and H. Weinfurter, Phys. Rev. Lett. **98**, 063604 (2007).
- [10] D. B. Hume, C. W. Chou, T. Rosenband, and D. J. Wineland, Phys. Rev. A **80**, 052302 (2009).
- [11] E. B. Treacy, Phys. Lett. A **27**, 421 (1968).
- [12] N. V. Vitanov, T. Halfmann, B. W. Shore, and K. Bergmann, Annu. Rev. Phys. Chem. **52**, 763 (2001).
- [13] C. Wunderlich, T. Hannemann, T. Körber, H. Häffner, C. Roos, W. Hänsel, R. Blatt, and F. Schmidt-Kaler, J. Mod. Opt. **54**, 1541 (2007).
- [14] J. R. Morris and B. W. Shore, Phys. Rev. A **27**, 906 (1983).
- [15] A. A. Rangelov, N. V. Vitanov, and B. W. Shore, Phys. Rev. A **74**, 053402 (2006).
- [16] A. Retzker, E. Solano, and B. Reznik, Phys. Rev. A **75**, 022312 (2007).
- [17] K. Toyoda, S. Haze, R. Yamazaki, and S. Urabe, Phys. Rev. A **81**, 032322 (2010).
- [18] H. Häffner, S. Gulde, M. Riebe, G. Lancaster, C. Becher, J. Eschner, F. Schmidt-Kaler, and R. Blatt, Phys. Rev. Lett. **90**, 143602 (2003).
- [19] A. Messiah, *Quantum mechanics*, Vol. 2 (North-Holland, 1961).
- [20] C. A. Sackett, D. Kielpinski, B. E. King, C. Langer, V. Meyer, C. J. Myatt, M. Rowe, Q. A. Turchette, W. M. Itano, D. J. Wineland, and I. C. Monroe, Nature **404**, 256 (2000).

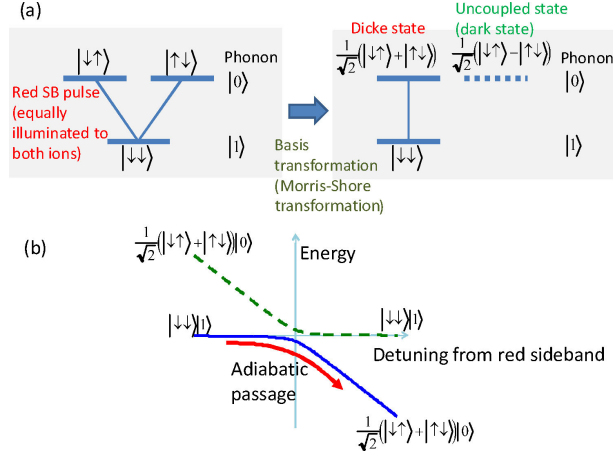


FIG. 1: (Color online) Basic concept for generating Dicke states using rapid adiabatic passage. (a) (left) Relevant states. A motional Fock state  $|\downarrow\downarrow\rangle|1\rangle$  is coupled to  $|\downarrow\uparrow\rangle|0\rangle$  and  $|\uparrow\downarrow\rangle|0\rangle$  with a red sideband pulse. (right) After applying a basis transformation (Morris–Shore transformation) to the upper two states, the system is decomposed into a two-state system and an uncoupled (dark) state. (b) Dressed state potentials for the two-state system plotted against the detuning of the laser from the red sideband resonance. In rapid adiabatic passage, the ions move from the left along the potential (indicated by the solid curve) to  $|D_2^{(1)}\rangle|0\rangle = (1/\sqrt{2})(|\downarrow\uparrow\rangle + |\uparrow\downarrow\rangle)|0\rangle$ . Here, the Rabi frequencies are assumed to be constant for simplicity, while it is usually varied in actual experiments.

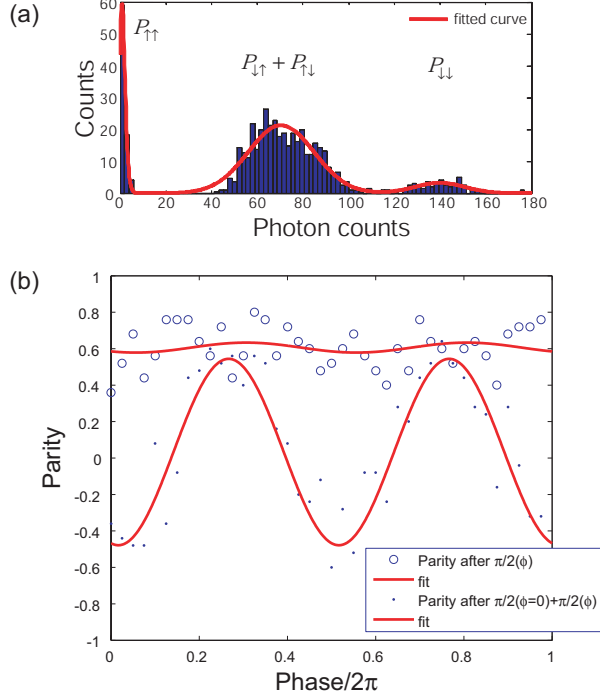


FIG. 2: (Color online) (a) Result of projection (population) measurement after Dicke state generation. A histogram of fluorescence counts obtained by shining a 397-nm laser beam for 7 ms after the generation of a Dicke state is shown. The left, middle, and right peaks (around 0, 70, and 140 counts, respectively) correspond to  $P_{\uparrow\uparrow}$ ,  $P_{\downarrow\uparrow} + P_{\uparrow\downarrow}$ , and  $P_{\downarrow\downarrow}$ , respectively, where  $P_{s_1 s_2}$  ( $s_1, s_2 = \downarrow, \uparrow$ ) represents the population in the respective basis state. From this,  $\rho_{\downarrow\uparrow, \downarrow\uparrow} + \rho_{\uparrow\downarrow, \uparrow\downarrow} = 0.74 \pm 0.06$  is obtained. (b) Result of parity measurement after Dicke state generation. The measured parity after Dicke state generation followed by the application of a  $\pi/2$  pulse is plotted against the phase of the  $\pi/2$  pulse phase (open circles). The solid curve is a sinusoidal fit with period  $\pi$  to the measured values. From this,  $2\text{Re}(\rho_{\downarrow\uparrow, \uparrow\downarrow}) = 0.58 \pm 0.02$  is obtained. Filled circles represent parities after Dicke state generation followed by two  $\pi/2$  pulses and the phase of the second pulse is variable. The sinusoidal oscillation with period  $\pi$  indicates the presence of  $(1/\sqrt{2})(|\downarrow\downarrow\rangle + |\uparrow\uparrow\rangle)$  after the first  $\pi/2$  pulse.

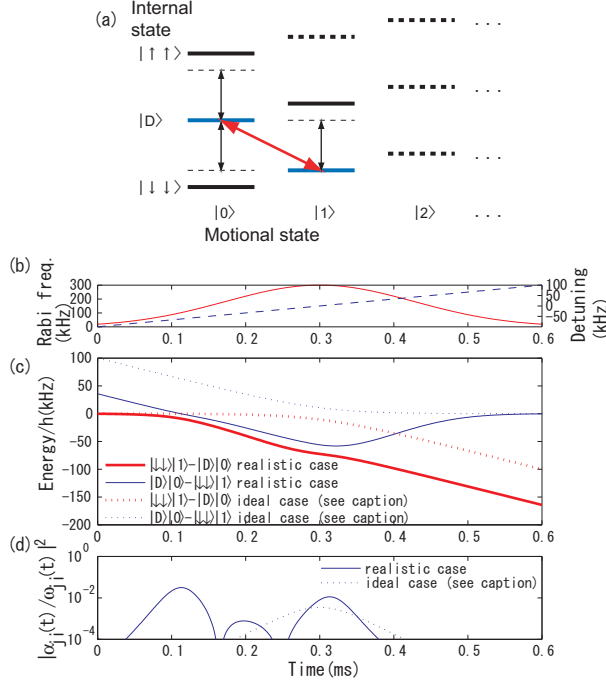


FIG. 3: (Color online) Effects of AC Stark shifts due to optical pulses for rapid adiabatic passage. (a) Energy levels used for the calculation (horizontal solid lines).  $|D\rangle$  represents  $|D_2^{(1)}\rangle = (1/\sqrt{2})(|\downarrow\uparrow\rangle + |\uparrow\downarrow\rangle)$ . The bold arrow indicates the transition used for rapid adiabatic passage and the other arrows represent couplings considered here for calculating the AC Stark shifts. (b) Variation of the envelope (solid curve) and detuning (dashed line) of an optical pulse for rapid adiabatic passage against time. The envelope is assumed to be a Gaussian function, and the detuning is assumed to be linear. (c) Variation of adiabatic energies of relevant levels against time (solid curves). They approach each other near 0.11 ms, as well as near 0.3 ms. The dashed curves are shown for comparison; they represent adiabatic energies for an ideal case in which Hamiltonian matrix elements for carrier transitions ( $|\downarrow\downarrow\rangle|1\rangle - |D\rangle|1\rangle$ ,  $|D\rangle|0\rangle - |\downarrow\downarrow\rangle|0\rangle$ ,  $|D\rangle|0\rangle - |\uparrow\uparrow\rangle|0\rangle$ ) are set to be zero. These potentials only approach each other near 0.3 ms. (d)  $|\alpha_{ji}(t)/\omega_{ji}(t)|^2$  indicating violation of adiabaticity is plotted (see text).

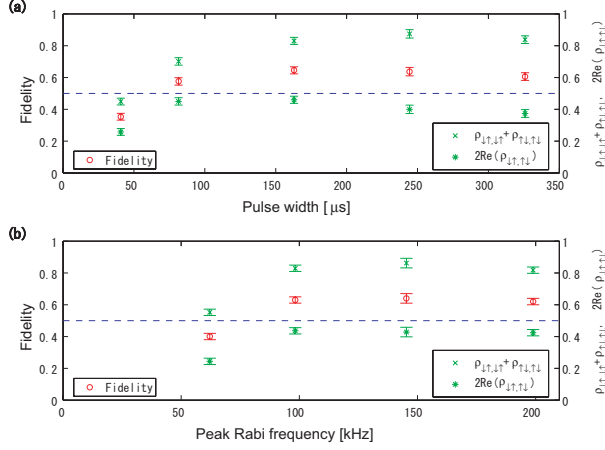


FIG. 4: (Color online) Verification of robustness in generation of Dicke states using rapid adiabatic passage. Gaussian pulses producing time-dependent Rabi frequency  $\Omega(t) = \Omega_{\text{peak}} \exp[-t^2/2\sigma^2]$  are applied as RAP pulses and values of obtained fidelity (circles) are estimated, with (a) the pulse width  $2\sigma$  and (b) the peak Rabi frequency  $\Omega_{\text{peak}}/2\pi$  varied. Here, the Rabi frequency is for the carrier transition.  $\Omega_{\text{peak}}/2\pi$  is fixed to 145 kHz in (a) and  $2\sigma$  is fixed to 244  $\mu\text{s}$  in (b). The total duration of each RAP pulse is 2.36 times the pulse width  $2\sigma$ , and during the pulse duration the excitation laser is swept from  $-100$  kHz below to 100 kHz above the resonance of the red sideband transition. The error bars represents 68% confidence intervals. The horizontal dashed lines at a fidelity of 0.5 represent the threshold for inseparable states (see text). Crosses and asterisks indicate values of  $\rho_{\downarrow\uparrow,\uparrow\downarrow} + \rho_{\uparrow\downarrow,\downarrow\uparrow}$  and  $2\text{Re}(\rho_{\downarrow\uparrow,\uparrow\downarrow})$ , respectively, which are used for discussions about infidelity in §VII